Reduced SV2A and GABA$_A$ receptor levels in the brains of type 2 diabetic rats revealed by [^{18}F]SDM-8 and [^{18}F]flumazenil PET

Kong, Yanyan ; Cao, Lei ; Xie, Fang ; Wang, Xiuzhe ; Zuo, Chuantao ; Shi, Kuangyu ; Rominger, Axel ; Huang, Qi ; Xiao, Jianfei ; Jiang, Donglang ; Guan, Yihui ; Ni, Ruiqing

DOI: https://doi.org/10.1016/j.biopha.2024.116252

Other titles: Reduced SV2A and GABAA receptor levels in the brains of type 2 diabetic rats revealed by [18F]SDM-8 and [18F]flumazenil PET

Posted at the Zurich Open Repository and Archive, University of Zurich
ZORA URL: https://doi.org/10.5167/uzh-256931
Journal Article
Published Version

Originally published at:
Kong, Yanyan; Cao, Lei; Xie, Fang; Wang, Xiuzhe; Zuo, Chuantao; Shi, Kuangyu; Rominger, Axel; Huang, Qi; Xiao, Jianfei; Jiang, Donglang; Guan, Yihui; Ni, Ruiqing (2024). Reduced SV2A and GABA$_A$ receptor levels in the brains of type 2 diabetic rats revealed by [^{18}F]SDM-8 and [^{18}F]flumazenil PET. Biomedicine Pharmacotherapy, 172:116252.
DOI: https://doi.org/10.1016/j.biopha.2024.116252

Biomedicine & Pharmacotherapy 172 (2024) 116252

Contents lists available at ScienceDirect

Biomedicine & Pharmacotherapy

journal homepage: www.elsevier.com/locate/biopha

Reduced SV2A and $GABA_A$ receptor levels in the brains of type 2 diabetic rats revealed by [^{18}F]SDM-8 and [^{18}F]flumazenil PET

Yanyan Kong [a,1], Lei Cao [a,b,1,2], Fang Xie [a], Xiuzhe Wang [c], Chuantao Zuo [a], Kuangyu Shi [d], Axel Rominger [d], Qi Huang [a], Jianfei Xiao [a], Donglang Jiang [a], Yihui Guan [a,*], Ruiqing Ni [b,d,e,**]

[a] PET Center, Huashan Hospital, Fudan University, Shanghai, China
[b] Inst. Regenerative Medicine, University of Zurich, Zurich, Switzerland
[c] Dept. Neurology, Shanghai Sixth People's Hospital affiliated with Shanghai Jiao Tong University School of Medicine, Shanghai, China
[d] Dept. Nuclear Medicine, Inselspital, Bern University Hospital, Bern, Switzerland
[e] Inst. Biomedical Engineering, University of Zurich & ETH Zurich, Zurich, Switzerland

ARTICLE INFO

Keywords:
Amyloid-beta
$GABA_A$ receptor
SV2A
Tau
Type 2 diabetes mellitus

ABSTRACT

Purpose: Type 2 diabetes mellitus (T2DM) is associated with a greater risk of Alzheimer's disease. Synaptic impairment and protein aggregates have been reported in the brains of T2DM models. Here, we assessed whether neurodegenerative changes in synaptic vesicle 2 A (SV2A), γ-aminobutyric acid type A ($GABA_A$) receptor, amyloid-β, tau and receptor for advanced glycosylation end product (RAGE) can be detected in vivo in T2DM rats.
Methods: Positron emission tomography (PET) using [^{18}F]SDM-8 (SV2A), [^{18}F]flumazenil ($GABA_A$ receptor), [^{18}F]florbetapir (amyloid-β), [^{18}F]PM-PBB3 (tau), and [^{18}F]FPS-ZM1 (RAGE) was carried out in 12-month-old diabetic Zucker diabetic fatty (ZDF) and Sprague—Dawley (SD) rats. Immunofluorescence staining, Thioflavin S staining, proteomic profiling and pathway analysis were performed on the brain tissues of ZDF and SD rats.
Results: Reduced cortical [^{18}F]SDM-8 uptake and cortical and hippocampal [^{18}F]flumazenil uptake were observed in 12-month-old ZDF rats compared to SD rats. The regional uptake of [^{18}F]florbetapir and [^{18}F]PM-PBB3 was comparable in the brains of 12-month-old ZDF and SD rats. Immunofluorescence staining revealed Thioflavin S-negative, phospho-tau-positive inclusions in the cortex and hypothalamus in the brains of ZDF rats and the absence of amyloid-beta deposits. The level of $GABA_A$ receptors was lower in the cortex of ZDF rats than SD rats. Proteomic analysis further demonstrated that, compared with SD rats, synaptic-related proteins and pathways were downregulated in the hippocampus of ZDF rats.
Conclusion: These findings provide in vivo evidence for regional reductions in SV2A and $GABA_A$ receptor levels in the brains of aged T2DM ZDF rats.

1. Introduction

T2DM is a major public health concern associated with a greater risk of brain damage, cognitive decline and susceptibility to AD [1]. Decreased hippocampal volume and long-term potentiation and changes in glucose metabolism have been observed in T2DM patients [2]. Post-mortem studies of the brains of patients with T2DM have demonstrated the loss of synaptic proteins and neurotransmitters, including γ-aminobutyric acid type A ($GABA_A$) receptors [3]. Studies in T2DM mouse and rat models have demonstrated metabolic alterations, $GABA_A$ receptor alterations [4], impairment in memory and learning, and hippocampal synaptic reorganization [5–7]. GABA is the main inhibitory neurotransmitter released at GABAergic synapses and plays an important role in regulating brain activity [3]. The beneficial effect of upregulating $GABA_A$ receptors was demonstrated in T2DM animal models [4]. In addition, advanced glycation end products (AGEs)/RAGE signaling plays an important role in T2DM and is involved in multiple pathways [8]. In addition, increased levels of soluble/insoluble amyloid-beta (Aβ),

* Correspondence to: 518 East Wuzhong Road, Shanghai, 200235 China.
** Correspondence to: Wagistrasse 12 9th floor, 8952 Zurich, Switzerland.
E-mail addresses: guanyihui@hotmail.com (Y. Guan), ruiqing.ni@uzh.ch (R. Ni).
[1] Equal contribution
[2] Currently working at Changes tech Co. Ltd.

https://doi.org/10.1016/j.biopha.2024.116252
Received 11 September 2023; Received in revised form 19 December 2023; Accepted 2 February 2024
Available online 6 February 2024

phospho-tau deposits, which are pathological features of the brains of AD patients and animal models, have been reported in the brains of T2DM rats [9–11].

PET imaging for Aβ and tau aggregates has been utilized in AD research and clinical settings to noninvasively map the regional distribution of these pathologies in the brain; such as [^{18}F]florbetapir, [^{18}F]florbetaben, [^{18}F]flutemetamol, and [^{11}C]PIB for the visualization of Aβ deposits; and [^{18}F]PI-2620, [^{18}F]flortaucipir [12–17], [^{18}F]MK-6240, [^{18}F]THK-5351, [^{18}F]RO948, [^{18}F]PM-PBB3 (APN-1607), and [^{11}C]PBB3 [18–22] for detection of tau inclusions. SV2A imaging using [^{18}F]SDM-8 ([^{18}F]SynVesT-1), [^{18}F]SDM-16, [^{18}F]UCB-H, and [^{11}C]UCB-J has enabled the in vivo detection of reduced synaptic density in the brain of AD patients and AD rodent models [23–27]. For mapping $GABA_A$ receptors, [^{11}C]flumazenil is the most widely-used tracer in both animal models and patients with various diseases [28]. Decreased cerebral uptake of [^{11}C]flumazenil has been demonstrated in AD patients and in the P301L tau mouse model [29]. However, the development of ligands for RAGE has been challenging. Several tracers that detect the extracellular domain of RAGE have been developed: including [^{18}F]FPS-ZM1 ([^{18}F]RAGER), [^{11}C]FPS-ZM1, [^{18}F]S100A4, [^{99m}Tc]anti--RAGE-F(ab′)$_2$, [^{64}Cu]Rho-G4-CML, [^{64}Cu]MMIA-CML, and [^{64}Cu]MMIA-HSA nanoparticles [30–35].

Here, we aimed to assess the levels of synaptic vesicle 2 A (SV2A), $GABA_A$ receptor, Aβ, tau, and RAGE by in vivo imaging in a widely-used T2DM model. Multitrace PET was performed using [^{18}F]SDM-8 (SV2A) [25], [^{18}F]flumazenil ($GABA_A$ receptor) [28], [^{18}F]florbetapir (Aβ), [^{18}F]PM-PBB3 (tau), and [^{18}F]FPS-ZM1 (RAGE) [30] in aged diabetic ZDF and SD rats, followed by immunofluorescence staining (for Aβ, tau, SV2A, $GABA_A$ receptor), Thioflavin S staining, proteomics and pathway analysis of hippocampal tissue.

2. Materials and methods

2.1. Animal models

Animal models, including 12-month-old ZDF rats, 12-month-old Sprague—Dawley (SD) rats, and 1.5-month-old C57BL/6 J mice, were used in the study (Table 1). The rats and mice were housed in ventilated cages inside a temperature-controlled room under a 12-h dark/light cycle. Pelleted food and water were provided ad libitum. Paper tissue and shelters were placed in cages for environmental enrichment. The in vivo PET imaging and experimental protocol was approved by the Institutional Animal Care and Ethics Committee of Fudan University and performed in accordance with the National Research Council's Guide for the Care and Use of Laboratory Animals and the ARRIVE guidelines 2.0,

2.2. Radiosynthesis

[^{18}F]SDM-8 (0.37 GBq/mL) [25] (**SFig. 1**) and [^{18}F]flumazenil (0.37 GBq/mL) [28] (**SFig. 2**) were synthesized as described earlier. [^{18}F]PM-PBB3 (1.48 GBq/mL) was synthesized from an automatic synthesis module and kit provided by APRINOIA therapeutics (Suzhou, China) [36]. [^{18}F]florbetapir (0.56 GBq/mL) was radiosynthesized from its precursor in a fully automated procedure suitable for routine clinical application [37,38]. [^{18}F]FPS-ZM1 (N-benzyl-4-chloro-N-cyclohexylbenzamide, 30 mCi/mL) was radiosynthesized from its precursor, as described in detail in the Supplementary file (**SFig. 3**) [30]. The identities of the standard precursor [^{18}F]FPS-ZM1 were confirmed by using mass spectrometry (MS), nuclear magnetic resonance (NMR) spectroscopy and high-performance liquid chromatography (HPLC; **SFigs. 4–7, STables 1, 2)**. The identities of the final products were confirmed by comparison with the HPLC retention times of the nonradioactive reference compounds by coinjection through the use of a Luna 5 μm C18(2) 100 Å (250 mm × 4.6 mm) column (Phenomenex) with acetonitrile and water (60:40) as the solvent and a 1.0 mL/min flow rate. Radiochemical purity > 95% was achieved for all the aforementioned tracers.

2.3. MicroPET

PET experiments using [^{18}F]SDM-8, [^{18}F]flumazenil, [^{18}F]florbetapir, [^{18}F]PM-PBB3 and [^{18}F]FPS-ZM1 were performed using a Siemens Inveon PET/CT system (Siemens Medical Solutions, Knoxville, United States) [39]. Prior to the scans, the rats were anaesthetized using isoflurane (1.5%) in medical oxygen (0.3–0.5 L/min) at room temperature with an isoflurane vaporizer (Molecular Imaging Products Company, USA). The rats were positioned in a spread-up position on the heated imaging bed and subjected to inhalation of the anaesthetic during the PET/computed tomography (CT) procedure. The temperature of the rats was monitored. A single dose of tracers (~0.37 MBq/g body weight, 0.2–0.5 mL) was injected into the animals through the tail vein under isoflurane anaesthesia. Static PET/CT images were obtained 10 min after intravenous administration of the tracer [^{18}F]SDM-8 at 60 min [25], [^{18}F]flumazenil at 20 min, [^{18}F]FPS-ZM1 at 90 min, [^{18}F]florbetapir at 50 min and [^{18}F]PM-PBB3 at 90 min [38]. PET/CT images were reconstructed using the ordered subsets expectation maximization 3D algorithm (OSEM3D), with 2 iterations, image zoom 1, matrix size of 128 × 128 × 159 and a voxel size of 0.815 mm × 0.815 mm× 0.796 mm. Data were reviewed using Inveon Research Workplace (IRW) software (Siemens). Attenuation corrections derived from hybrid CT data were applied.

2.4. Biodistribution study

To evaluate the biodistribution of [^{18}F]FPS-ZM1, 54 mice (aged 1.5 months, 27 M, 27 F) were intravenously injected with [^{18}F]FPS-ZM1 (140 μCi) via the tail vein. Six animals (3 M, 3 F) were euthanized at each time point: 2 min, 5 min, 10 min, 15 min, 30 min, 45 min, 1 h, 3 h, and 4 h post injection. The organs and brain regions of the mice were dissected, weighed and analysed for radioactivity using a gamma counter (**STable. 4**). Blood sampling was performed on six mice (3 M, 3 F) at 2 min, 5 min, 10 min, 15 min, 30 min, 45 min, 1 h, 2 h, 3 h, and 4 h post injection.

2.5. Imaging data analysis

The images were processed and analysed using PMOD 4.4 software (PMOD Technologies Ltd., Zurich, Switzerland). Radioactivity is presented as the standardized uptake value (SUV) (decay-corrected radioactivity per cm^3 divided by the injected dose per gram body weight) [40]. The time−activity curves were deduced from specific volumes of

Table 1
Information on the rats and mice used in the study.

Rat	Sex	Age (month)	[^{18}F] SDM-8	[^{18}F] flumazenil	[^{18}F] FPS-ZM1	[^{18}F] florbetapir	[^{18}F] PM-PBB3	Staining
SD	M	12	4	3	1	8	4	3
ZDF	M	12	5	3	5	15	7	8
Mouse	**Sex**	**Age (month)**	**Biodistri-bution**	**Blood sampling**				
C57BL/6 J	M	1.5	27	3				
C57BL/6 J	F	1.5	27	3				

M, male; F, female: mice were used for [^{18}F]FPS-ZM1 biodistribution and blood sampling

interest that were defined based on a rat MRI T_2-weighted image template (W. Schiffer). The brain regional SUVRs were calculated using the cerebellum (CB) as the reference region. A mask was applied for signals outside the brain volumes of interest for illustration (**SFig. 8**).

2.6. Immunofluorescence staining and Thioflavin S staining

After in vivo imaging, 8 ZDF and 3 SD rats were transcardially perfused under deep anaesthesia (pentobarbital sodium 50 mg/kg body weight, i.p. bolus injection) with ice-cold 0.1 M phosphate buffered saline (PBS, pH 7.4) and 4% paraformaldehyde (PFA) in 0.1 M PBS (pH 7.4). The brains were extracted from the skull and fixed for 24 h in 4% PFA and then stored in 0.1 M PBS at 4 °C. For immunofluorescence analysis, coronal rat brain Section (3 μm) were cut at approximately bregma − 3.24 mm and 5.76 mm from the ZDF and SD rat brains [41] using Rm2016 Leica Microtome (Leica Microsystems). After antigen retrieval in citrate buffer at room temperature, the sections were permeabilized and blocked in 3% bovine Serum Albumin for 30 min at room temperature with mild shaking. The sections were incubated overnight at 4 °C with primary antibodies (**STable. 3**) against Aβ40, phospho-Tau (Ser202/Thr205), SV2A and $GABA_A$ alpha-1 receptor as described earlier [42]. The next day, the slices were washed with PBS 3 × 5 min and incubated with a suitable secondary antibody for 50 min at room temperature (**STable. 3**). Sections were washed 3 × 5 min with PBS. For Thioflavin S staining, the slices were incubated in filtered 1% Thioflavin S solution for 8 min at room temperature. The sections were washed 2 × 3 min in 80% ethanol and 3 min in 95% ethanol, followed by 3 washes using distilled water. The brain sections were incubated for 10 min in 4′,6-diamidino-2-phenylindole (DAPI) at room temperature and mounted with antifade mounting media. The brain sections were imaged at × 20 magnification using a Panoramic MIDI slide scanner (3DHISTECH) using the same acquisition settings for all brain slices. The images were analysed by using ImageJ (NIH, U.S.A.). The levels of SV2A and $GABA_A$ receptors were determined by measuring the mean fluorescence intensity in the hippocampus and in the cortex [42].

2.7. Proteomic profiling and pathway analysis

After in vivo imaging, high-throughput quantitative proteomics analysis was performed on hippocampal samples from two 12-month-old ZDF rats and two age-matched SD rats using tandem mass tag (TMT) labelling (**STables 1, 2**). Hippocampal rat brain tissues were collected and homogenized on ice for 10 min in lysis buffer containing 4% sodium dodecyl sulfate (SDS), 7 mM urea, 30 mM N-2-hydroxyethylpiperazine-N′− 2-ethanesulfonic acid (HEPES), 1 mM phenylmethylsulfonyl fluoride (PMSF), 2 mM ethylenediaminetetraacetic acid (EDTA), 2 mM thiourea, 10 mM DL-dithiothreitol (DTT), and 1 × protease inhibitor. The supernatant was centrifuged at 10000g for 30 min at 4 °C. The supernatant was then incubated with 100 mM tetraethylammonium bromide (TEAB) and 10 mM DTT for 60 min at 55 °C, 35 mM iodoacetamide was added for 60 min in the dark, and 5 times acetonitrile (v/v) was added at − 20 °C for 3 h. The sample was centrifuged at 20000g for 30 min at 4 °C. The remaining sample was then incubated twice with 1 mL of 50% acetonitrile at − 20 °C for 3 h and centrifuged at 20000g for 30 min at 4 °C. Then, 0.1 mL of 100 mM TEAB was added to the protein precipitate and mixed. The peptide/protein concentration was determined using the bicinchoninic acid (BCA) protein assay. The protein precipitate was added to 100 μL of 100 mM TEAB, 1 mg/mL trypsin, and 1.0 mg of enzyme/100 mg of protein and incubated at 37 °C for 4 h. Then, trypsin (1.0 mg) was added, followed by incubation at 37 °C for 12 h. The peptide solution was centrifuged at 5,000g and dried into powder using a freeze dryer. The enzymatic hydrolysis efficiency was detected using LC—MS. The peptide/protein concentration in the supernatant was determined by BCA protein assay.

TMT labelling of peptides was performed according to the instructions of the TMT 6-plex kit. Peptides were analysed using an LC system. Extracted spectra from Proteome Discoverer (2.4.0.305) were searched with Sequest HT. Quantitative analysis of the spectra resulting from the first step was performed using Proteome Discoverer. The false positive rate (FDR) was set at ≤ 1% for both the protein and peptide levels (p value <0.05; fold change >1.2).

In addition, a comprehensive bioinformatics analysis was used to investigate the differentially expressed proteins and enriched signaling pathways as described earlier [43–45]. We analysed the differentially expressed genes (DEPs) by using principal component analysis (PCA), volcano plot analysis, subcellular localization analysis, cluster of orthologous groups of proteins (COG) analysis, kinase analysis, proteomic and peptide assays, Kyoto Encyclopedia of Genes and Genomes (KEGG) signalling pathways, modification site assays, differential gene expression analysis, and gene ontology (GO) analysis. KEGG signaling pathway analysis was performed using the database for *Rattus norvegicus* (rat) (www.kegg.jp/kegg/pathway.html). GO analysis was performed using the GO database (http://www.geneontology.org/) with annotations based on the UniProt database (https://www.uniprot.org/taxonomy/10116). Protein—protein interaction (PPI) network analysis was performed for the DEPs using the STRING database for *Rattus norvegicus* (rat) (v11, stringdb.org).

2.8. Statistics

Two-way ANOVA with Sidak's post hoc analysis was used for comparisons between groups (GraphPad Prism 9.0, CA, USA). Pearson correlation analysis was used to analyse the associations between the regional SUVRs of different tracers. $p < 0.05$ indicated statistical significance. The data are shown as the mean ± standard deviation.

3. Results

3.1. No detectable differences in amyloid-β or tau PET uptake in the brain of ZDF compared to SD rats

We observed comparable levels of [^{18}F]florbetapir (ZDF rat, n = 15; SD rat, n = 8; Fig. 1**a-c**) and [^{18}F]PM-PBB3 (ZDF rat, n = 7; SD rat, n = 4; Fig. 1**d-f**) in the brains of 12-month-old ZDF and SD rats. These findings suggested that there was no apparent accumulation of aggegated Aβ or tau deposits in the brains of ZDF rats at 12 months of age. To validate the in vivo observation of negative amyloid-beta and tau PET results in the ZDF rats, *ex vivo* staining was performed using antibodies against $Aβ_{40}$ and phospho-Tau as well as using Thioflavin S on the brain tissues from 8 ZDF and 3 SD rats after in vivo scanning. No specific signals for $Aβ_{40}$ deposits were observed across the brain slices from ZDF rats (Fig. 1**g, j, k**). Positive phospho-Tau inclusions were observed in the cortex (layer 2/3) and in the hypothalamus but not in the hippocampus of ZDF rats (Fig. 1**h, l-n**). We further found that there was no specific Thioflavin S signal in the brain tissue slices from ZDF rats, even though positive phospho-Tau inclusions were detected in the cortex (Fig. 1**i, o**). No specific signals for $Aβ_{40}$ deposits, phospho-Tau or Thioflavin S were observed in brain tissue slices from SD rats (not shown).

3.2. Reduced regional levels of SV2A and $GABA_A$ receptors in ZDF rat brains

Next, we assessed the synaptic alterations in the brain of ZDF rats by in vivo imaging of SV2A and $GABA_A$ receptors. The level of SV2A revealed by [^{18}F]SDM-8 was lower in the parietal cortex of 12-month-old ZDF rats than in age-matched SD rats (p = 0.0087, ZDF rat, n = 5; SD rat, n = 4; Fig. 2**a-c**). The [^{18}F]flumazenil SUVR, indicative of $GABA_A$ receptor level, was reduced by approximately 30% in the frontal cortex (p = 0.0015), approximately 25% in the somatosensory cortex (p = 0.0244) and approximately 30% in the hippocampus (anterior dorsal p = 0.0092, posterior p = 0.0417) of 12-month-old ZDF rats

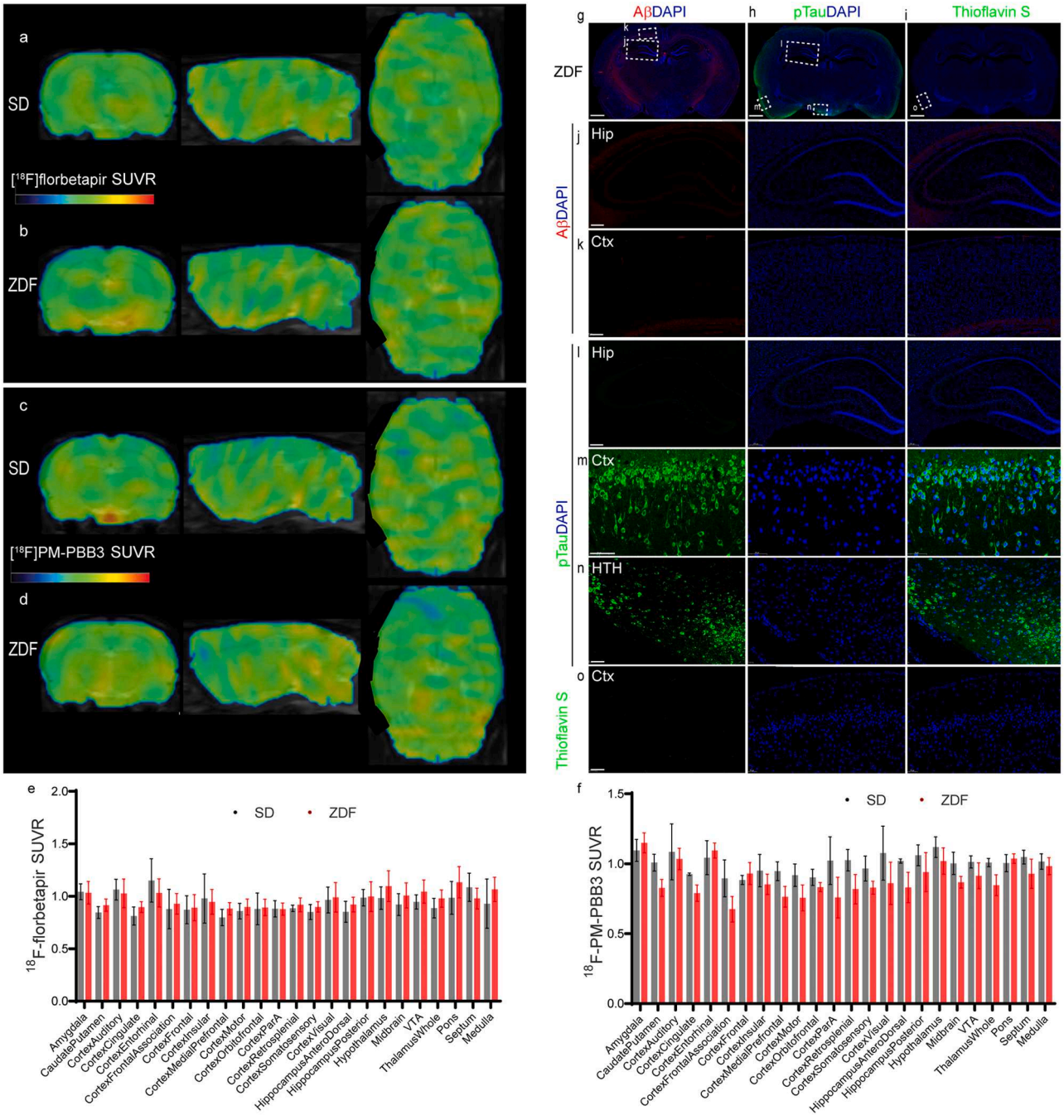

Fig. 1. No detectable changes in amyloid-beta or tau levels caused by [^{18}F] florbetapir or [^{18}F] PM-PBB3 brain uptake in 12-month-old ZDF rats compared to age-matched SD rats. (a-b) [^{18}F]florbetapir and (c-d) [^{18}F]PM-PBB3 SUVR images (scale 0–2.2). (e-f) Quantification of [^{18}F]florbetapir SUVRs in the brain (ZDF rats, n = 15; SD rats, n = 8) and [^{18}F]PM-PBB3 (ZDF rats, n = 7; SD rats, n = 4). (g-o) Representative images of coronal brain slices from ZDF rats showing amyloid-beta (Aβ, red), phospho-tau (p-Tau, green), and Thioflavin S (green) expression. An overview and zoomed-in view of the staining of the cortex (Ctx), hippocampus (Hip) and hypothalamus (HTH) revealed the presence of Thioflavin S-negative, p-Tau-positive inclusions in the Ctx and HTH of ZDF rats. Nuclei were counterstained with DAPI (blue). Scale bar = 1 mm (g-i) or 50 μm (j-o).

compared to age-matched SD rats (ZDF rats, n = 3; SD rats, n = 3; Fig. 2**d-f**). To validate the in vivo observation of alterations in SV2A and $GABA_A$ levels in the brains of ZDF rats compared to SD rats, ex vivo staining was performed using anti-SV2A and anti- $GABA_A$ antibodies on brain tissues from ZDF and SD rats after in vivo imaging. The level of SV2A in the cortex and hippocampus did not differ between ZDF rats (n = 8) and SD rats (n = 3) (Fig. 2**g-j, o**). A reduced level of $GABA_A$ receptor was observed in the cortex of ZDF rats (n = 8) compared to SD rats (n = 3), but not in the hippocampus (Fig. 2**k-n, p**).

3.3. *Proteomic profiling and pathway analysis*

A total of 309 DEPs were detected in the hippocampi of 12-month-old ZDF rats compared to those of SD rats; these DEPs were mainly annotated as cytoplasmic (38.57%) or periplasmic (34.08%) (Fig. 3**b,** Table S1). The changes in the levels of SV2A, Aβ, Tau, MAPT, and GABAA were not significantly different. The list of DEPs was included in the Supplement datasheet. Downregulated proteins, including the synaptic-related proteins Dbnl, Syn1, Syn2, and Map2, were detected (Fig. 3**a**). The DEPs were mostly associated with signal transduction

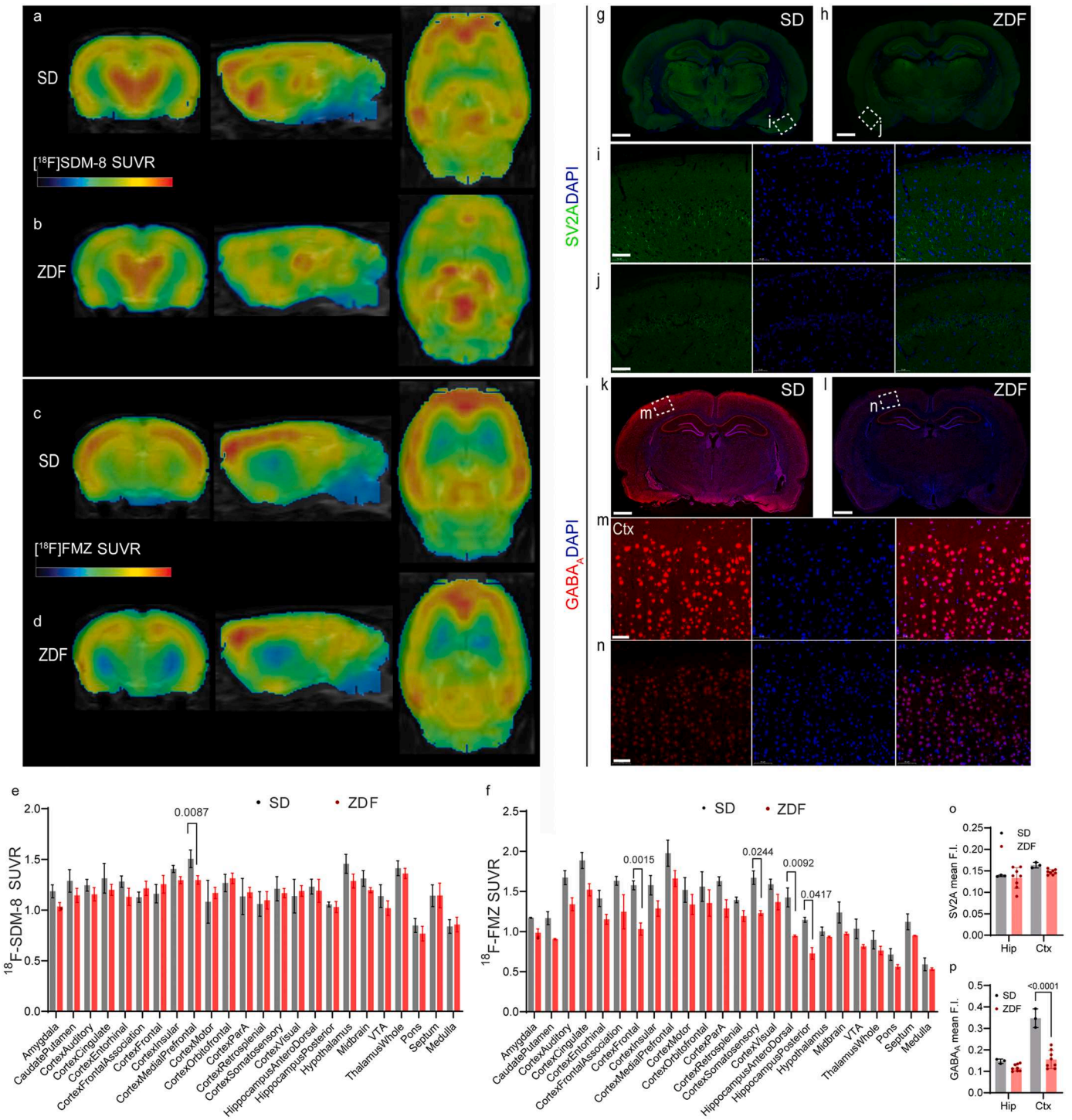

Fig. 2. Decreased regional levels of SV2A and $GABA_A$ receptors in the brains of 12-month-old ZDF rats compared to those in the brains of age-matched SD rats. (a-b) [^{18}F]SDM-8 and (c-d) [^{18}F]flumazenil (FMZ) SUVR images (scale 0–2.2). (e, f) Quantification of [^{18}F]SDM-8 SUVRs in the brain (ZDF rat, n = 5; SD rat, n = 4) and [^{18}F]FMZ (ZDF rat, n = 3; SD rat, n = 3). (g-n) Representative coronal images of SV2A (red) and $GABA_A$ receptor (green) staining in brain slices from ZDF and SD rats. Overview (g, h, k, l) and zoom-in view of staining of the cortex (Ctx) (i, j, m, n). (o-p) Quantification of the levels of SV2A and $GABA_A$ receptors in the cortex and hippocampus (Hip) of ZDF rats (n = 8) compared to those in SD rats (n = 3). Nuclei were counterstained with DAPI (blue). Scale bars = 1 mm (g, h, k, l) and 50 μm (i, j, m, n).

mechanisms and enriched in synapse and neuron signaling (Fig. 3**c, d**). Enrichment analysis of the DEPs indicated enrichment in the MAPK and cAMP insulin secretion-related pathways, endocrine and other factor-regulated calcium reabsorption pathways, etc. (Fig. 4**a**). The protein—protein interaction network visualized the alterations with the proteins shown as nodes (Fig. 4**b, c**).

3.4. Large variation in [^{18}F]FPS-ZM1 uptake in the brains of ZDF rats

We first assessed the biodistribution of RAGE tracer [^{18}F]FPS-ZM1 in mice. High variation in [^{18}F]FPS-ZM1 levels in various brain regions and high liver uptake were observed by ex vivo biodistribution in C57BL/6 J mice (**SFig. 9a-c**). Next we asessed the tracer performance in ZDF and

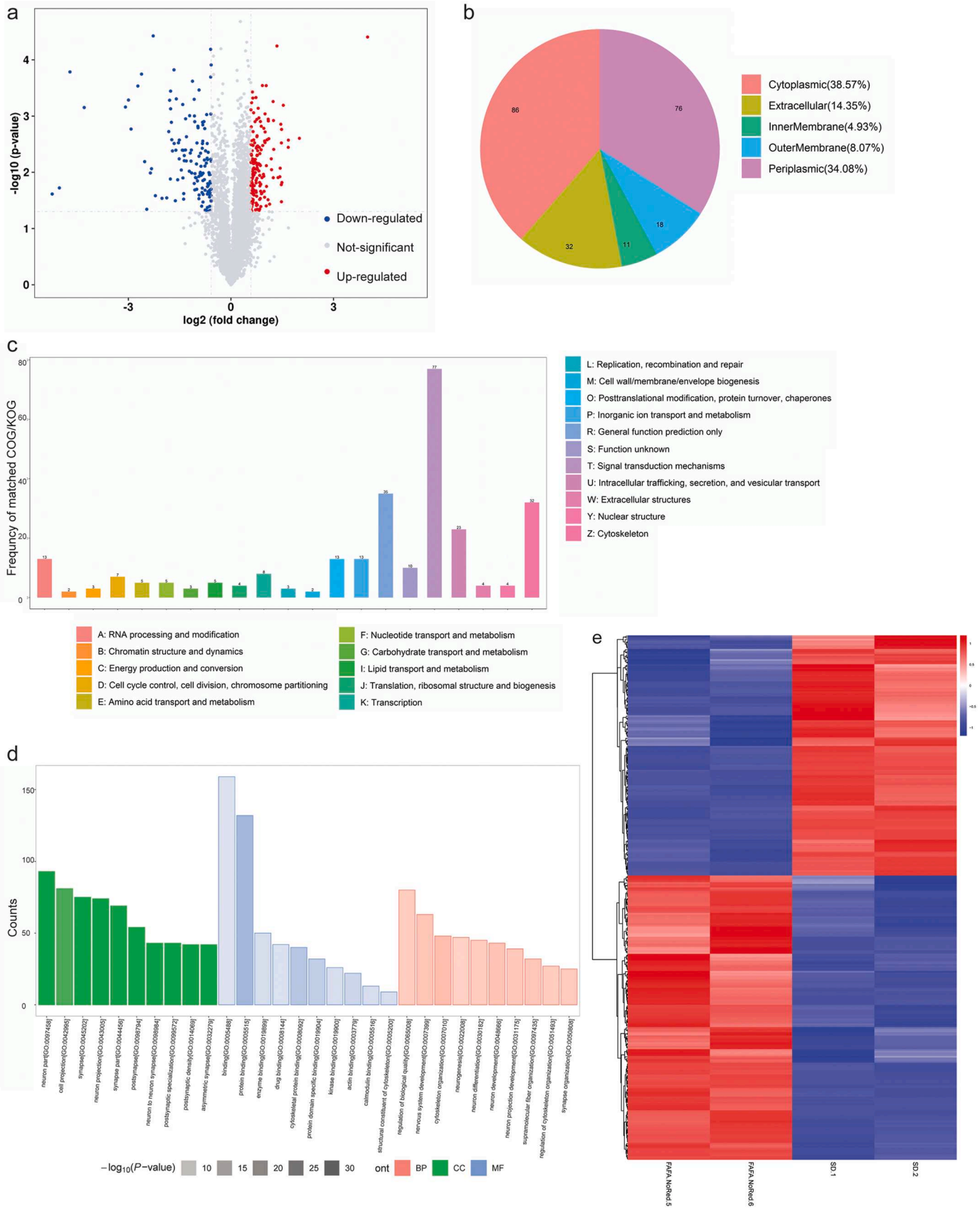

Fig. 3. Profiling of differentially expressed proteins (DEPs) in the hippocampus of 12-month-old ZDF and SD rats. (a) Volcano plots showing the log2-fold change (x-axis) and -log10 p value (y-axis) for all quantified proteins. (b) Location of DEPs. (c) The number of matched genes assigned to clusters of orthologous groups (COGs) and eukaryotic orthologous groups (KOGs). (d) Gene Ontology (GO) enrichment analysis of biological process (BP), cellular component (CC), and molecular function (MF) terms. The number on the x-axis indicates the enrichment count of DEPs. (e) Heatmap of DEPs.

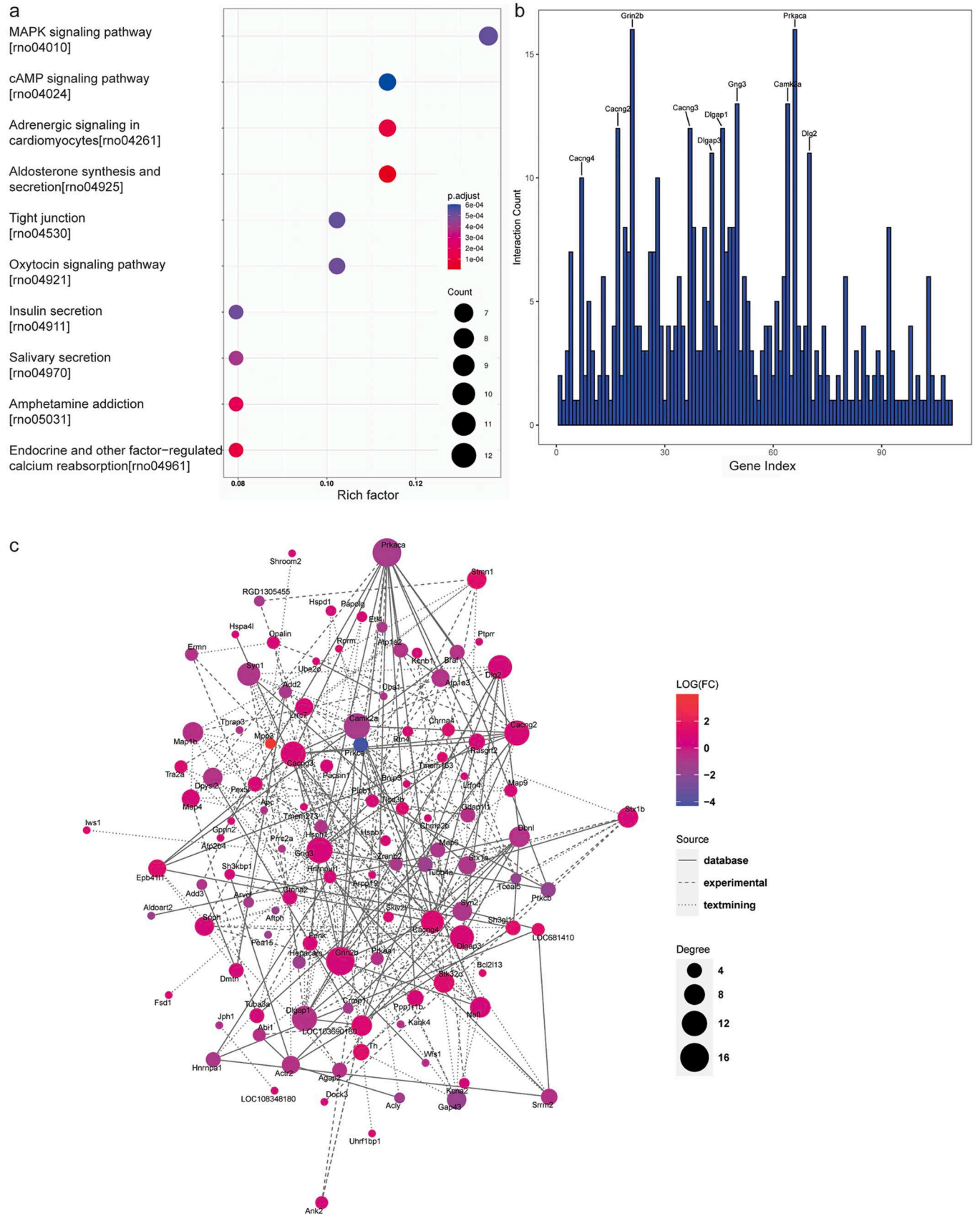

Fig. 4. Kyoto Encyclopedia of Genes and Genomes (KEGG) pathway analysis of the pathways associated with the differentially expressed proteins (DEPs). (a) Enrichment analysis showing the top 10 enriched pathway terms. (b, c) Protein—protein interaction network analysis. Histogram of interactions (b). The proteins present in the networks are shown as nodes (c).

SD rats. The brain uptake of [^{18}F]FPS-ZM1 was lower in the brain than in the spinal cord and in the upper trunk in 12-month-old ZDF rats (**SFigs. 9d-g**). Large variations in the regional distribution of RAGE in the brains of 12-month-old ZDF rats determined by PET using [^{18}F]FPS-ZM1 were also observed.

4. Discussion

Thus far, few imaging studies have reported alterations in the central nervous system in T2DM models, including [^{18}F]FP-CMT for dopamine innervation [46] and [^{18}F]FDG for glucose metabolism. Cognitive impairment, cortical thinning, and hippocampal synaptic reorganization have been observed in T2DM rats [6]. Here, we demonstrated synaptic and GABAergic impairments without detectable changes in the levels of Aβ or tau by PET in the brains of 12-month-old ZDF rats compared to SD rats. To our knowledge, this is the first study that visualized these targets noninvasively in the brain of T2DM animal models.

One possibility for the lack of differences in the levels of [^{18}F]florbetapir and [^{18}F]PM-PBB3 uptake could be that the accumulation levels of Aβ and tau deposits have not reached the threshold detectable or that the aggregates did not contain sufficient fibrillar structures for the β-sheet binding imaging tracers to recognize [47,48]. Our *ex vivo* immunofluorescence staining showed the presence of positive phospho-Tau inclusions in the layer 2/3 cortex as well as in the hypothalamus, and lack of Aβ deposits in the brains of ZDF rats of 12-month--old ZDF rats. In addition, these deposits were not Thioflavin S-positive and thus not detectable by the β-sheet-binding amyloid or tau PET tracers. The observation of tau inclusions was in line with earlier study showing p-Tau, and Silver staining-positive tau inclusions in the brain of ZDF rats [9]. Although positive Aβ immunohistochemical staining in the brain of ZDF rats has been shown earlier, beta-sheet rich Aβ aggregates has not been reported [10,11]. The level of these protein aggregates in the brain appeared much lower compared to animal models of tauopathy [49–51] and amyloidosis [42], where positive in vivo imaging data were obtained.

Our finding of mildly reduced cortical levels of SV2A measured by [^{18}F]SDM-8 in the brains of aged ZDF rats compared to SD rats corroborated our findings of the downregulation of synaptic-related proteins Dbnl, Syn1, Syn2, and Map2, and synaptic-related pathways in the hippocampal tissues from 12-month-old ZDF rats compared to SD rats. This finding is in line with earlier biochemical [5–7], and proteomic studies in the hippocampus of ZDF rats that revealed reduced levels of the metalloprotein apolipoprotein C, myelin-binding protein and apolipoprotein A-I as well as the synaptic proteins Mapk1, OMG, Gng12, Dbnl, and Stx12 [43–45]. Our *ex vivo* immunofluorescence staining of SV2A on the brain slices and proteomic analysis of the hippocampus tissue did not show significant change comparing the ZDF and SD rats. Reduction in the level of SV2B, but not SV2A and SV2C has been reported earlier in the brain of obese zucker rats compared to lean zucker rats [52]. Another proteomic study showed a higher level of SV2A (1.24x) in the brain of SD rats compared to ZDF rats [45].

Our observation of reduced [^{18}F]flumazenil uptakes ($GABA_A$ receptors) in the cortex and hippocampus of aged ZDF rats compared to SD rats corroborated with the *ex vivo* immunofluorescence staining results of reduced cortical level of $GABA_A$ α1 receptors in the brains of ZDF rats. This result is also in line with the known alterations in $GABA_A$ receptors in the brain of ZDF rats [4]. Given the important role of the GABAergic system in diabetic-related cognitive dysfunction, blood sugar control and energy homeostasis [53], the GABAergic system has been an important drug target for treating T2DM. Therefore, [^{18}F]flumazenil might be useful in further investigations and monitoring of therapeutics targeting GABAergic impairment in T2DM patients.

Autoradiography using [^{11}C]FPS-ZM1 in aged Tg2576 amyloidosis mice [31], as well as [^{18}F]InRAGER (intracellular domain of RAGE) in a lipopolysaccharide model, has been reported [54]. However, the relatively suboptimal affinity (15 nM), high lipophilicity (CLogP: 5.25), and rapid metabolism of [^{18}F]FPS-ZM1 limit its in vivo performance [30]. Our biodistribution, pharmacokinetic and in vivo [^{18}F]FPS-ZM1 PET results in ZDF rats are in line with earlier observations [54]. Further optimization of tracers targeting RAGE is needed for in vivo application.

This study has several limitations. Firstly, only male ZDF and SD rats at 12 months of age were investigated. Further imaging studies including both male and female rats at different ages and at different stages of disease are needed. Secondly, we did not include lean zucker rats for comparison with ZDF rats. In addition, we performed the biodistribution study of the tracer [^{18}F]FPS-ZM1 for RAGE in mice but not in rats. Moreover, PET using [^{18}F]FMZ measures synaptic $GABA_A$ receptor, mainly the alpha1 subtype.Other subtypes and extra-synaptic $GABA_A$ receptor were not measured in the current study and therefore remain to be evaluated.

In summary, we demonstrated regional reductions in SV2A and $GABA_A$ receptor levels in the brains of aged ZDF rats in vivo, without detectable Aβ or tau accumulation by PET. Further study using a balanced and longitudinal design will provide further insights into the dynamics of SV2A and $GABA_A$ receptor alterations in the brains of T2DM rats, for understanding cognitive impairment in T2DM.

Ethics approval

The PET imaging and experimental protocol were approved by the Institutional Animal Care and Ethics Committee of Fudan University and performed in accordance with the National Research Council's Guide for the Care and Use of Laboratory Animals.

Authors' contributions

The study was designed by KY and RN. KY and QH performed the radiolabelling. KY performed HPLC and microPET. KY, LC and RN performed the microPET analysis, staining and microscopy analysis. KY, LC and RN interpreted the data. CZ, JD, and JX prepared the tracers. KY, LC and RN wrote the first draft. All the authors contributed to the revision of the manuscript and approved the final manuscript.

Funding

YK received funding from the National Natural Science Foundation of China (NSFC, 82272108, 81701732), the Natural Science Foundation of Shanghai (22ZR1409200) and the Shanghai Science and Technology Innovation Action Plan Medical Innovation Research Project (23Y11903200). YG received funding from the NSFC (82071962). RN received funding from the Swiss Center for Advanced Human Toxicity (SCAHT-AP22_01).

CRediT authorship contribution statement

Xiao Jianfei: Data curation, Investigation, Writing – review & editing. **Guan Yihui:** Funding acquisition, Resources, Writing – review & editing. **Ni Ruiqing:** Conceptualization, Formal analysis, Funding acquisition, Project administration, Resources, Supervision, Visualization, Writing – original draft, Writing – review & editing. **Kong Yanyan:** Conceptualization, Data curation, Funding acquisition, Investigation, Writing – original draft, Project administration, Software, Writing – review & editing. **Cao Lei:** Formal analysis, Investigation, Visualization, Writing – review & editing. **Xie Fang:** Resources, Writing – review & editing. **Wang Xiuzhe:** Writing – review & editing. **Zuo Chuantao:** Methodology, Writing – review & editing. **Shi Kuangyu:** Writing – review & editing. **Rominger Axel:** Resources, Writing – review & editing. **Huang Qi:** Investigation, Writing – review & editing. **Jiang Donglang:** Investigation, Methodology.

Declaration of Competing Interest

The authors declare that they have no known competing financial interests or personal relationships that could have appeared to influence the work reported in this paper.

Data availability

Data will be made available on request.

Appendix A. Supporting information

Supplementary data associated with this article can be found in the online version at doi:10.1016/j.biopha.2024.116252.

References

[1] M.S. Beeri, B.B. Bendlin, The link between type 2 diabetes and dementia: from biomarkers to treatment, Lancet Diabetes Endocrinol. 8 (9) (2020) 736–738.
[2] G.J. Biessels, F. Nobili, C.E. Teunissen, R. Simó, P. Scheltens, Understanding multifactorial brain changes in type 2 diabetes: a biomarker perspective, Lancet Neurol. 19 (8) (2020) 699–710.
[3] W. Koh, H. Kwak, E. Cheong, C.J. Lee, GABA tone regulation and its cognitive functions in the brain, Nat. Rev. Neurosci. 24 (9) (2023) 523–539.
[4] L.L. Tu, Q. Sun, L.L. Wei, J. Shi, J.P. Li, Upregulation of GABA receptor promotes long-term potentiation and depotentiation in the hippocampal CA1 region of mice with type 2 diabetes mellitus, Exp. Ther. Med. 18 (4) (2019) 2429–2436.
[5] A. Kamal, G.M. Ramakers, W.H. Gispen, G.J. Biessels, Hyperinsulinemia in rats causes impairment of spatial memory and learning with defects in hippocampal synaptic plasticity by involvement of postsynaptic mechanisms, Exp. Brain Res. 226 (1) (2013) 45–51.
[6] A.M. Magariños, B.S. McEwen, Experimental diabetes in rats causes hippocampal dendritic and synaptic reorganization and increased glucocorticoid reactivity to stress, Proc. Natl. Acad. Sci. USA 97 (20) (2000) 11056–11061.
[7] J. Zhang, L. Liu, Y. Zhang, Y. Yuan, Z. Miao, K. Lu, X. Zhang, R. Ni, H. Zhang, Y. Zhao, et al., ChemR23 signaling ameliorates cognitive impairments in diabetic mice via dampening oxidative stress and NLRP3 inflammasome activation, Redox Biol. 58 (2022) 102554.
[8] J. Chaudhuri, Y. Bains, S. Guha, A. Kahn, D. Hall, N. Bose, A. Gugliucci, P. Kapahi, The role of advanced glycation end products in aging and metabolic diseases: bridging association and causality, Cell Metab. 28 (3) (2018) 337–352.
[9] F. Talaei, V.M. Van Praag, M.H. Shishavan, S.W. Landheer, H. Buikema, R. H. Henning, Increased protein aggregation in Zucker diabetic fatty rat brain: identification of key mechanistic targets and the therapeutic application of hydrogen sulfide, BMC Cell Biol. 15 (1) (2014).
[10] T. Bi, L. Zhang, L. Zhan, R. Feng, T. Zhao, W. Ren, T. Hang, W. Zhou, X. Lu, Integrated analyses of microbiomics and metabolomics explore the effect of gut microbiota transplantation on diabetes-associated cognitive decline in zucker diabetic fatty rats, Front Aging Neurosci. 14 (2022) 913002.
[11] Z.G. Li, W. Zhang, A.A. Sima, Alzheimer-like changes in rat models of spontaneous diabetes, Diabetes 56 (7) (2007) 1817–1824.
[12] S. Rojas, J.R. Herance, J.D. Gispert, S. Abad, E. Torrent, X. Jiménez, D. Pareto, U. Perpiña, S. Sarroca, E. Rodríguez, et al., In vivo evaluation of amyloid deposition and brain glucose metabolism of 5XFAD mice using positron emission tomography, Neurobiol. Aging 34 (7) (2013) 1790–1798.
[13] H. Kroth, F. Oden, J. Molette, H. Schieferstein, F. Capotosti, A. Mueller, M. Berndt, H. Schmitt-Willich, V. Darmency, E. Gabellieri, et al., Discovery and preclinical characterization of [(18)F]PI-2620, a next-generation tau PET tracer for the assessment of tau pathology in Alzheimer's disease and other tauopathies, Eur. J. Nucl. Med Mol. Imaging 46 (10) (2019) 2178–2189.
[14] W.E. Klunk, H. Engler, A. Nordberg, Y. Wang, G. Blomqvist, D.P. Holt, M. Bergström, I. Savitcheva, G.-F. Huang, S. Estrada, et al., Imaging brain amyloid in Alzheimer's disease with Pittsburgh compound-B, : Ann. Neurol. vol. 55 (2004) 306–319.
[15] A. Rominger, M. Brendel, S. Burgold, K. Keppler, K. Baumann, G. Xiong, E. Mille, F. J. Gildehaus, J. Carlsen, J. Schlichtiger, et al., Longitudinal assessment of cerebral β-amyloid deposition in mice overexpressing Swedish mutant β-amyloid precursor protein using 18F-florbetaben PET, J. Nucl. Med 54 (7) (2013) 1127–1134.
[16] A. Snellman, J. Rokka, F.R. Lopez-Picon, O. Eskola, I. Wilson, G. Farrar, M. Scheinin, O. Solin, J.O. Rinne, M. Haaparanta-Solin, Pharmacokinetics of [^{18}F] flutemetamol in wild-type rodents and its binding to beta amyloid deposits in a mouse model of Alzheimer's disease, Eur. J. Nucl. Med Mol. Imaging 39 (11) (2012) 1784–1795.
[17] D.R. Schonhaut, C.T. McMillan, S. Spina, B.C. Dickerson, A. Siderowf, M.D. Devous, R. Sr., Tsai, J. Winer, D.S. Russell, I. Litvan, et al., 18) F-flortaucipir tau positron emission tomography distinguishes established progressive supranuclear palsy from controls and Parkinson disease: a multicenter study, Ann. Neurol. 82 (4) (2017) 622–634.
[18] K. Tagai, M. Ono, M. Kubota, S. Kitamura, K. Takahata, C. Seki, Y. Takado, H. Shinotoh, Y. Sano, Y. Yamamoto, et al., High-contrast in vivo imaging of Tau pathologies in Alzheimer's and non-Alzheimer's disease tauopathies, Neuron 109 (1) (2021) 42–58, e48.
[19] R. Ossenkoppele, R. Smith, N. Mattsson-Carlgren, C. Groot, A. Leuzy, O. Strandberg, S. Palmqvist, T. Olsson, J. Jögi, E. Stormrud, et al., Accuracy of Tau Positron Emission Tomography as a Prognostic Marker in Preclinical and Prodromal Alzheimer Disease: A Head-to-Head Comparison Against Amyloid Positron Emission Tomography and Magnetic Resonance Imaging, JAMA Neurol 78 (8) (2021) 961–971.
[20] T.J. Betthauser, P.J. Lao, D. Murali, T.E. Barnhart, S. Furumoto, N. Okamura, C. K. Stone, S.C. Johnson, B.T. Christian, In vivo comparison of tau radioligands 18F-THK-5351 and 18F-THK-5317, J. Nucl. Med. 58 (6) (2017) 996–1002.
[21] E.D. Hostetler, A.M. Walji, Z. Zeng, P. Miller, I. Bennacef, C. Salinas, B. Connolly, L. Gantert, H. Haley, M. Holahan, et al., Preclinical Characterization of 18 F-MK-6240, a Promising PET Tracer for In Vivo Quantification of Human Neurofibrillary Tangles, J Nucl. Med. 57 (10) (2016) 1599–1606.
[22] R. Ni, B. Ji, M. Ono, N. Sahara, M.R. Zhang, I. Aoki, A. Nordberg, T. Suhara, M. Higuchi, Comparative in vitro and in vivo quantifications of pathologic tau deposits and their association with neurodegeneration in tauopathy mouse models, J. Nucl. Med. 59 (6) (2018) 960–966.
[23] C. Zheng, D. Holden, M.Q. Zheng, R. Pracitto, K.C. Wilcox, M. Lindemann, Z. Felchner, L. Zhang, J. Tong, K. Fowles, et al., A metabolically stable PET tracer for imaging synaptic vesicle protein 2A: synthesis and preclinical characterization of [(18)F]SDM-16, Eur. J. Nucl. Med Mol. Imaging 49 (5) (2022) 1482–1496.
[24] M. Naganawa, S. Li, N. Nabulsi, S. Henry, M.Q. Zheng, R. Pracitto, Z. Cai, H. Gao, M. Kapinos, D. Labaree, et al., First-in-Human Evaluation of (18)F-SynVesT-1, a Radioligand for PET Imaging of Synaptic Vesicle Glycoprotein 2A, J. Nucl. Med 62 (4) (2021) 561–567.
[25] S. Li, Z. Cai, X. Wu, D. Holden, R. Pracitto, M. Kapinos, H. Gao, D. Labaree, N. Nabulsi, R.E. Carson, et al., Synthesis and in vivo evaluation of a novel PET radiotracer for imaging of synaptic vesicle glycoprotein 2A (SV2A) in nonhuman primates, ACS Chem. Neurosci. 10 (3) (2019) 1544–1554.
[26] M.A. Bahri, A. Plenevaux, J. Aerts, C. Bastin, G. Becker, J. Mercier, A. Valade, T. Buchanan, N. Mestdagh, D. Ledoux, et al., Measuring brain synaptic vesicle protein 2A with positron emission tomography and [18F]UCB-H, Alzheimer'S. Dement.: Transl. Res. Clin. Interv. 3 (4) (2017) 481–486.
[27] D. Bertoglio, J. Verhaeghe, A. Miranda, I. Kertesz, K. Cybulska, Š. Korat, L. Wyffels, S. Stroobants, L. Mrzljak, L. Liu, et al., Validation and noninvasive kinetic modeling of [11C]UCB-J PET imaging in mice, J. Cereb. Blood Flow. Metab. 40 (2019), 0271678×1986408.
[28] X. Zhang, F. Basuli, R.E. Swenson, An azeotropic drying-free approach for copper-mediated radiofluorination without addition of base, J. Label. Comp. Radio. 62 (3) (2019) 139–145.
[29] M. Shimojo, H. Takuwa, Y. Takado, M. Tokunaga, S. Tsukamoto, K. Minatohara, M. Ono, C. Seki, J. Maeda, T. Urushihata, et al., Selective disruption of inhibitory synapses leading to neuronal hyperexcitability at an early stage of tau pathogenesis in a mouse model, J. Neurosci. 40 (17) (2020) 3491–3501.
[30] B.P. Cary, A.F. Brooks, M.V. Fawaz, L.R. Drake, T.J. Desmond, P. Sherman, C. A. Quesada, P.J. Scott, Synthesis and evaluation of [(18)F]RAGER: a first generation small-molecule PET radioligand targeting the receptor for advanced glycation endproducts, ACS Chem. Neurosci. 7 (3) (2016) 391–398.
[31] F. Luzi, V. Savickas, C. Taddei, S. Hader, N. Singh, A.D. Gee, S. Bongarzone, Radiolabeling of [(11)C]FPS-ZM1, a receptor for advanced glycation end products-targeting positron emission tomography radiotracer, using a [(11)C]CO(2)-to-[(11)C]CO chemical conversion, Future Med. Chem. 12 (6) (2020) 511–521.
[32] C.J. Konopka, M. Wozniak, J. Hedhli, A. Ploska, A. Schwartz-Duval, A. Siekierzycka, D. Pan, G. Munirathinam, I.T. Dobrucki, L. Kalinowski, et al., Multimodal imaging of the receptor for advanced glycation end-products with molecularly targeted nanoparticles, Theranostics 8 (18) (2018) 5012–5024.
[33] Y. Tekabe, J. Luma, A.J. Einstein, M. Sedlar, Q. Li, A.M. Schmidt, L.L. Johnson, A novel monoclonal antibody for RAGE-directed imaging identifies accelerated atherosclerosis in diabetes, J. Nucl. Med 51 (1) (2010) 92–97.
[34] S. Wolf, C. Haase-Kohn, J. Lenk, S. Hoppmann, R. Bergmann, J. Steinbach, J. Pietzsch, Expression, purification and fluorine-18 radiolabeling of recombinant S100A4: a potential probe for molecular imaging of receptor for advanced glycation endproducts in vivo? Amino Acids 41 (4) (2011) 809–820.
[35] M. Woźniak, C.J. Konopka, A. Płoska, J. Hedhli, A. Siekierzycka, M. Banach, R. Bartoszewski, L.W. Dobrucki, L. Kalinowski, I.T. Dobrucki, Molecularly targeted nanoparticles: an emerging tool for evaluation of expression of the receptor for advanced glycation end products in a murine model of peripheral artery disease, : Cell Mol. Biol. Lett. 26 (1) (2021) 10.
[36] K. Kawamura, H. Hashimoto, K. Furutsuka, T. Ohkubo, T. Fujishiro, T. Togashi, D. Arashi, T. Sakai, M. Muto, M. Ogawa, et al., Radiosynthesis and quality control testing of the tau imaging positron emission tomography tracer [(18) F]PM-PBB3 for clinical applications, J. Label. Comp. Radio. 64 (3) (2021) 109–119.
[37] Y. Liu, L. Zhu, K. Plössl, S.R. Choi, H. Qiao, X. Sun, S. Li, Z. Zha, H.F. Kung, Optimization of automated radiosynthesis of [18F]AV-45: a new PET imaging agent for Alzheimer's disease, Nucl. Med Biol. 37 (8) (2010) 917–925.
[38] Y. Kong, C.A. Maschio, X. Shi, B. Yao, F. Xie, C. Zuo, U. Konietzko, K. Shi, A. Rominger, J. Xiao, et al., Relationship between reactive astrocytes, by [18F] SMBT-1 imaging, with amyloid-beta, tau, glucose metabolism, and microgliosis in mouse models of Alzheimer's disease, bioRxiv (2023), https://doi.org/10.1101/2023.08.21.554163.
[39] Y. Kong, L. Huang, W. Li, X. Liu, Y. Zhou, C. Liu, S. Zhang, F. Xie, Z. Zhang, D. Jiang, et al., The synaptic vesicle protein 2A interacts with key pathogenic factors in Alzheimer's disease: implications for treatment, Front. Cell Dev. Biol. 9 (2021) 609908.

[40] R. Ni, A. Müller Herde, A. Haider, C. Keller, G. Louloudis, M. Vaas, R. Schibli, S. M. Ametamey, J. Klohs, L. Mu, In vivo Imaging of Cannabinoid Type 2 Receptors: Functional and Structural Alterations in Mouse Model of Cerebral Ischemia by PET and MRI, Mol. Imaging Biol. 24 (2022) 700–709.
[41] G. Paxinos, C. Watson, The rat brain in stereotaxic coordinates: hard cover edition, Elsevier, 2006.
[42] V. Kecheliev, L. Boss, U. Maheshwari, U. Konietzko, A. Keller, D. Razansky, R. M. Nitsch, J. Klohs, R. Ni, Aquaporin 4 is differentially increased and dislocated in association with tau and amyloid-beta, Life Sci. 321 (2023) 121593.
[43] S.M. Nam, D.Y. Yoo, H.J. Kwon, J.W. Kim, H.Y. Jung, D.W. Kim, H.J. Han, M. H. Won, J.K. Seong, I.K. Hwang, et al., Proteomic approach to detect changes in hippocampal protein levels in an animal model of type 2 diabetes, Neurochem Int 108 (2017) 246–253.
[44] S. Wang, Z. Lu, Y. Wang, T. Zhang, X. He, Metalloproteins and apolipoprotein C: candidate plasma biomarkers of T2DM screened by comparative proteomics and lipidomics in ZDF rats, Nutr. Metab. (Lond.) 17 (2020) 66.
[45] H. Xu, W. Zhou, L. Zhan, H. Sui, L. Zhang, C. Zhao, X. Lu, The ZiBuPiYin recipe regulates proteomic alterations in brain mitochondria-associated ER membranes caused by chronic psychological stress exposure: Implications for cognitive decline in Zucker diabetic fatty rats, Aging 12 (23) (2020) 23698–23726.
[46] P. Cumming, S. Maschauer, P.J. Riss, E. Grill, M. Pischetsrieder, T. Kuwert, O. Prante, Perturbed development of striatal dopamine transporters in fatty versus lean zucker rats: a follow-up small animal PET study, Mol. Imaging Biol. 17 (4) (2015) 521–528.
[47] L. Cao, Y. Kong, B. Ji, Y. Ren, Y. Guan, R. Ni, Positron emission tomography in animal models of tauopathies, Front Aging Neurosci. 13 (2021) 761913.
[48] R. Ni, Positron emission tomography in animal models of Alzheimer's disease amyloidosis: translational implications, Pharmaceuticals 14 (11) (2021).
[49] R. Ni, Z. Chen, J.A. Gerez, G. Shi, Q. Zhou, R. Riek, K.P.R. Nilsson, D. Razansky, J. Klohs, Detection of cerebral tauopathy in P301L mice using high-resolution large-field multifocal illumination fluorescence microscopy, Biomed. Opt. Express 11 (9) (2020) 4989–5002.
[50] T. Sartoretti, R.P. Ganley, R. Ni, P. Freund, H.U. Zeilhofer, J. Klohs, Structural MRI reveals cervical spinal cord atrophy in the P301L mouse model of tauopathy: gender and transgene-dosing effects, Front. Aging Neurosci. 14 (2022) 825996.
[51] A. Ishikawa, M. Tokunaga, J. Maeda, T. Minamihisamatsu, M. Shimojo, H. Takuwa, M. Ono, R. Ni, S. Hirano, S. Kuwabara, et al., In vivo visualization of tau accumulation, microglial activation, and brain atrophy in a mouse model of tauopathy rTg4510, J. Alzheimers Dis. 61 (3) (2018) 1037–1052.
[52] I. Martinelli, D. Tomassoni, P. Roy, F. Amenta, S.K. Tayebati, Altered brain cholinergic and synaptic markers in obese Zucker rats, Cells 10 (10) (2021) 2528.
[53] H. Zhou, Z. Rao, Z. Zhang, J. Zhou, Function of the GABAergic system in diabetic encephalopathy, Cell Mol. Neurobiol. 43 (2) (2023) 605–619.
[54] L.R. Drake, A.F. Brooks, J. Stauff, P.S. Sherman, J. Arteaga, R.A. Koeppe, A. Reed, T.J. Montavon, M.B. Skaddan, P.J.H. Scott, Strategies for PET imaging of the receptor for advanced glycation endproducts (RAGE), J. Pharm. Anal. 10 (5) (2020) 452–465.